Pulsed squeezed-light generation in $\chi^{(2)}$ nonlinear waveguides

Matthew E. Anderson, D. F. McAlister, and M. G. Raymer

Oregon Center for Optics and Department of Physics, University of Oregon, Eugene, Oregon 97403

Mool C. Gupta

Imaging Research and Advanced Development, Eastman Kodak Company, Rochester, New York 14650-2017

Received January 21, 1997; revised manuscript received May 2, 1997

We present a brief history of experimental studies of quadrature squeezing, a tutorial on the physical origin and theory of squeezing, and our experimental study of squeezing by means of $\chi^{(2)}$ (second-order) nonlinear waveguides. We recently obtained 28% squeezing in quasi-phase-matched $LiTaO_3$ waveguides, using picosecond pulses. The amount of squeezing appears to be limited primarily by blue-light-induced red absorption.
 [S0740-3224(97)00211-7]

1. INTRODUCTION

Years after its first observation, squeezed light is still the premiere vehicle for demonstrating the importance of quantum mechanics in nonlinear optics; it is an inherently nonclassical light field that eludes explanation by classical physics. Current progress in squeezing is being fueled by advances in nonlinear devices and in measurement theory and techniques. In this paper we review the history and physics of squeezed light, discuss the advantages of generating squeezed light in optical waveguides, and present our experimental results on pulsed squeezing in quasi-phase-matched second-order nonlinear optical waveguides.

Quadrature field squeezing is a general concept that applies to electromagnetic signals with the measured variance of a particular quadrature amplitude lying below the corresponding shot-noise-limited variance associated with a coherent field. The conjugate quadrature amplitude undergoes an increase in variance beyond the shot-noise level. The motivation for applications of squeezed light originated with the idea that, when it is using the reduced variance of a squeezed signal, a measurement apparatus would be more sensitive than the standard quantum limit of an ordinary coherent state. The relatively modest amounts of squeezing obtained to date, though, combined with the huge amount of effort involved, have severely hampered fulfillment of squeezed light's anticipated capabilities. Fortunately, optical waveguides appear to offer a technique for easily generating large amounts of highly squeezed light.

2. CHRONOLOGY

The starting point for a discussion of the theoretical development of squeezed states originates with coherent states, originally alluded to by Schrödinger.[1] The impetus for a rigorous quantum-mechanical treatment of coherent electromagnetic states, however, lagged Schrödinger's notion by more than 30 years, until the advent of the laser and quantum optics. In the early 1960's Glauber[2] recognized that the traditional basis states used to describe the harmonic oscillator, the number states, were lacking in simplicity for describing the optical states of the laser. He developed the coherent state, an eigenstate of the annihilation operator, which has equal uncertainties in each quadrature. The quadrature amplitudes Q and P are the real and the imaginary parts, respectively, of the electric-field amplitude, $E \propto Q + iP$, and therefore represent the two phase components of the oscillating wave, that is, $\mathrm{Re}\, E \exp(-i\omega t) = Q \cos \omega t + P \sin \omega t$.

Subsequently, it was discovered that the coherent-state description was not, in fact, general enough. To describe states of unequal quadrature uncertainties required development of a new formalism. These new states, identified by a variety of names, eventually became known as squeezed states.[3] Building on studies by Louisell *et al.*,[4] who analyzed parametric processes, Takahasi[5] considered the use of squeezed states for optical communication in his quantum analysis of the parametric amplifier, calling them simply "wave packets." Squeezed states underwent further theoretical development by Stoler,[6] who showed that minimum-uncertainty packets can be obtained by unitary transformation of the coherent states. Yuen[7] formulated a complete theory of squeezing and solidified its position in the mainstream of quantum optics, referring to these states as "two-photon coherent states." Caves[8] proposed increasing the sensitivity of interferometers by injecting squeezed light.

In 1985 a team from Bell Laboratories[9] led by Slusher found the first experimental evidence of squeezing by using a four-wave mixing process induced by the $\chi^{(3)}$ nonlinear susceptibility of a sodium atomic beam. The amount of squeezing (25%) was modest. Soon thereafter squeezing was observed in several different media [$\chi^{(2)}$ and $\chi^{(3)}$] and geometries (traveling-wave, intracavity, op-

0740-3224/97/113180-11$10.00

Table 1. History of Experimental Quadrature Squeezing

Reference	System[a]	Squeezing (%)
9	$\chi^{(3)}$, Na beam	25
10	$\chi^{(3)}$, fiber	13
11	$\chi^{(2)}$, subthreshold OPO	63
12	$\chi^{(3)}$, Na vapor	4
13	$\chi^{(3)}$, Na beam	30
14	$\chi^{(3)}$, four-mode	20
15	$\chi^{(2)}$, subthreshold OPO	37
16	$\chi^{(2)}$, pulsed squeezing	13
17	$\chi^{(2)}$, frequency doubling	13
18	$\chi^{(2)}$, subthreshold OPO	55
19	$\chi^{(3)}$, Na vapor	25
20	$\chi^{(2)}$, incoherent pulse	17
21	$\chi^{(2)}$, frequency doubling	40
22	$\chi^{(2)}$, Josephson parametric amplifier	47
23	$\chi^{(2)}$, pulsed squeezing	22
24	$\chi^{(3)}$, optical solitons	32
25	$\chi^{(3)}$, pulsed squeezing	68
26	$\chi^{(3)}$, Na, single-beam	17
27	$\chi^{(2)}$, self-matched LO	37
28	$\chi^{(3)}$, Ba beam	18
29	$\chi^{(2)}$, OPO, SHG	40
30	$\chi^{(2)}$, mode-locked OPO	30
31	$\chi^{(2)}$, pulsed, type I	34
32	$\chi^{(2)}$, subthreshold OPO	75
33	$\chi^{(2)}$, whole-pulse detection	30
34	$\chi^{(3)}$, two-pulse, fiber	50
35	$\chi^{(3)}$, low-power, fiber	37
36	$\chi^{(3)}$, gigahertz pump, fiber	69
37	$\chi^{(2)}$, self-matched LO	74
38	$\chi^{(3)}$, semiconductor ZnS	40
39	$\chi^{(2)}$, KTP waveguide	12
40	$\chi^{(2)}$, $LiNbO_3$ waveguide	14
41	$\chi^{(2)}$, subthreshold OPO	72
42	$\chi^{(3)}$, semiconductor ZnSe	7
43	$\chi^{(3)}$, cold atoms	40
This work	$\chi^{(2)}$, $LiTaO_3$ waveguide	28

[a] OPO, optical parametric oscillator.

tical fibers). In Table 1 we present a (semicomplete) history of quadrature squeezing experiments, an extension of a list given earlier in a review by Kimble.[44] In the table we indicate the reference, the system that was used (where we allude to the novelty of each experiment), and the amount of squeezing, given in percent of intensity-noise variance below the shot-noise level, with 100% indicating perfect squeezing (zero noise).

3. OPTICAL WAVEGUIDES

The motivation for creating squeezed light by traveling-wave parametric amplification in waveguides is the potential to benefit from the high pump intensity that results from the transverse confinement and from the possibility of spatial mode control. In bulk crystals, several problems hamper the available gain. In the linear-gain (undepleted-pump) regime the diffractions of the pump and signal beams differ because of the differing wavelengths of the beams, so when the signal is created spontaneously in the pump waist volume it diffracts more strongly than does the pump. Furthermore, the two phase quadratures of the signal field experience different spatially dependent gains, leading to the introduction of additional modes along with an accompanying loss of squeezing (gain-induced diffraction).[37,45] There are also nonlinear mechanisms, including Kerr-lens [$\chi^{(3)}$] focusing,[26] that can affect the transverse spatial profile of the generated squeezed light. While these mechanisms limit the squeezing achievable in bulk media with no waveguiding, in a waveguide the transverse profile is determined largely by the step-index changes rather than by nonlinear optical index changes. The resulting mode control leads to more-efficient interaction between signal and pump fields and also produces a squeezed field in a well-defined spatial mode. Consequently, mode matching to a local-oscillator (LO) field, which is necessary to detect the squeezing, is easier.

The main difficulty encountered in early $\chi^{(3)}$ squeezing in optical-fiber waveguides was the presence of guided acoustic wave Brillouin scattering (GAWBS) noise. Thermal excitations in the fiber cause index-of-refraction modulations, which add phase-noise sidebands to the pump light and effectively suppress the squeezing process. Recently Bergman *et al.*[36] discovered a way to avoid GAWBS noise by using a high-repetition-rate short-pulse laser. If the repetition rate of the laser is higher than the GAWBS bandwidth, good squeezing can be obtained between the GAWBS spectral peaks if such peaks are fortuitously placed in frequency. Furthermore, the use of short pulses, as originally demonstrated by Slusher *et al.*[16] to increase peak power, helps to overcome the GAWBS problem because the GAWBS noise scales as the average power in the beam, whereas the squeezing scales with the peak power in the individual pulses. Ho *et al.*[46] have proposed $\chi^{(3)}$ squeezing in semiconductor waveguides below half-band-gap to further reduce these and other limitations. The observation of squeezing in a bulk semiconductor below half-band-gap by Fox *et al.*[38] is an encouraging step in this direction.

Squeezing in $\chi^{(2)}$ waveguides, in which the medium polarization is quadratic in the field strength, promises several advantages compared with $\chi^{(3)}$ waveguides, in which the polarization is cubic in the field. $\chi^{(2)}$ waveguides eliminate the masking of squeezing by GAWBS noise, since the squeezing appears at half the optical frequency of the pump. This phenomenon was first pointed out and studied theoretically by Kumar.[47] Furthermore, many materials have much higher $\chi^{(2)}$ than $\chi^{(3)}$ nonlinearity, which permits the use of a much shorter gain medium (1 cm, compared with tens of meters). A shorter medium leads to less GAWBS noise as well as to less self-phase modulation of the pulsed fields, another mechanism that degrades squeezing in $\chi^{(3)}$ media.[46] Nevertheless, there is a practical disadvantage in using $\chi^{(2)}$ media—the need to generate a LO field for detecting squeezing at one half the pump frequency. Efficient $\chi^{(2)}$ waveguide frequency doublers[48] can help solve this problem.

Methods for the generation of good amounts of squeezing seem to be well understood. The difficulty lies in the

detection of squeezing. High detection efficiency is essential to avoid losses of photons and thus of the correlations that give rise to squeezing.[44] There are several factors that go into overall detection efficiency, the first of which is the quantum efficiency of the detectors themselves. Currently available silicon photodiodes can have efficiencies approaching unity.[44] The second consideration in detection is mode matching between the signal and LO fields. Squeezed-field quadratures are measured by balanced-homodyne detection,[49,50] in which the squeezed beam is interfered with a reference (LO) beam and is then detected. Good spatial and temporal mode overlap is essential to facilitate the field interference that transfers the squeezing correlations of the signal into a reduction of noise on the LO. In a waveguide the spatial mode is defined by the waveguide itself; thus one can optimize the spatial mode matching, as Kumar originally pointed out, by passing the LO through an identical waveguide.[47]

When one is using pulses, the temporal mode overlap is slightly more complicated. It was predicted early on by Yurke *et al.*[51] that, to maximize the detected squeezing, the LO should be as short as possible to overlap the peak of the squeezed signal (see also Smithey *et al.*[52] and Ho *et al.*[46]). This theory was later refined by Werner *et al.*,[53] who included the less than infinite phase-matching bandwidth for squeezed-light generation. They found that for optimum squeezing detection the LO pulse should be shorter than the duration of the pump pulse that generates the squeezed light but not so short that its spectrum is wider than that of the squeezed field (which is usually determined by the phase-matching bandwidth). This point typically becomes significant only when ultrashort-pulse ($\lesssim$10-fs) lasers are used.[54] Werner *et al.* also describe how to tailor the temporal structure of the LO pulse to compensate for the linear dispersion that is present in the $\chi^{(2)}$ medium. LO compensation for nonlinear dispersion in a $\chi^{(3)}$ medium is discussed by Ho *et al.*[46]

Squeezing in $\chi^{(2)}$ waveguides was achieved recently[39] with ultrashort pulses in quasi-phase-matched KTP waveguides[55] and shortly thereafter in quasi-phase-matched $LiNbO_3$ waveguides by Serkland *et al.*[40] Quasi-phase matching (QPM) permits access to the large d_{33} [$d = \chi^{(2)}/2$] nonlinearity that cannot be utilized in crystals that are phase matched by birefringence (d_{33} requires that all fields be polarized in the same direction). Additionally, QPM makes accessible a wider range of wavelengths for parametric interactions than is found in the bulk case. Despite these advantages, several problems hampered each of these experiments, limiting the obtained squeezing to modest amounts (12% and 14%, respectively). In the former experiment the waveguides were not single mode, preventing proper spatial mode matching with the LO. In the latter, two-photon absorption (TPA) limited the pump energy and the squeezing gain. Both experiments confirmed the absence of gain-induced diffraction, however, removing one of squeezing's upper limits applicable in bulk media. Amplitude squeezing (15%) was recently demonstrated in quasi-phase-matched $LiNbO_3$ waveguides by means of traveling-wave second-harmonic generation[56] (SHG).

In the remainder of this paper we give a brief theoretical treatment of squeezing and present our recent experimental findings: 28% squeezing in quasi-phase-matched $LiTaO_3$ waveguides by use of picosecond pulses. We also discuss the limitations imposed by TPA of the blue pump and the associated blue-light-induced red absorption.

4. PHYSICS OF QUADRATURE SQUEEZING

Squeezed light has a rich history of theoretical treatment. Our presentation here is by no means intended to be exhaustive. We merely want to present some of the more subtle points of squeezing. For further consideration, a good tutorial is given by Loudon and Knight.[57] Here we present a derivation of quadrature squeezing arising from $\chi^{(2)}$ parametric amplification. The result that we obtain is equivalent to a result presented by Yurke *et al.*,[51] although our approach differs slightly in that Yurke *et al.* started from the nonlinear wave equation, whereas we identify the nonlinear Hamiltonian and proceed via Heisenberg's equation of motion. To preserve generality we approach the problem from a broadband starting point, then ultimately restrict our results to the narrowband approximation. We do this in an effort to shed light on the underlying quantum-mechanical nature of squeezed light, a phenomenon that is intimately intertwined with the production of pairs of photons.

Squeezing can arise from the nonlinear optical response of dielectric materials. In the analysis below, we follow the derivation given by Boyd,[58] generalizing it to quantized fields. A nonlinear medium is characterized by a polarization

$$\tilde{P} = \epsilon_0[\chi^{(1)}\tilde{E} + \chi^{(2)}\tilde{E}^2 + \chi^{(3)}\tilde{E}^3\ldots], \tag{1}$$

where $\tilde{P}$ is defined in SI units such that the nonlinear susceptibility $\chi^{(2)}$ is given in units of meters per volt [see Ref. 58, App. A]. The second-order susceptibility $\chi^{(2)}$ is responsible for second-harmonic generation and parametric amplification. The third-order susceptibility $\chi^{(3)}$ controls four-wave mixing and self-focusing. Here we derive an equation of motion for the degenerate parametric amplifier (in a type I process, in which all light fields near ω_s have the same polarization vector and propagate in the same transverse mode). A signal field with frequency near ω_s will interact with a pump field at frequency ω_p ($=2\omega_s$) through the second-order susceptibility $\chi^{(2)}$. For our derivation, however, we begin generally, writing the electric field as a sum of frequency modes. This approach will illustrate, we hope, the relationship between photon pairs. That is, a photon at frequency ω_m will be produced by a pump photon at ω_p only with the simultaneous production of another photon at $\omega_n = \omega_p - \omega_m$ (the nondegenerate case) to conserve energy ($\omega_m + \omega_n = \omega_p$). In the limit that $\omega_m \to \omega_p/2$, the two photons produced will have the same frequency (the degenerate case).

We can write the signal's electric field as

$$\begin{aligned}\tilde{E}_s(z, t) &= \hat{A}_s^{(+)}(z, t)\exp(-i\omega_s t)\exp(ik_s z) \\ &\quad + \hat{A}_s^{(-)}(z, t)\exp(i\omega_s t)\exp(-ik_s z) \\ &= \sum_{n=-\infty}^{\infty} \hat{E}(\omega_n)\exp(-i\omega_n t)\end{aligned} \tag{2}$$

and the monochromatic pump field as

$$\tilde{E}_p(z, t) = \hat{E}(\omega_p)\exp(-i\omega_p t) + \text{h.c.} \tag{3}$$

(the tilde indicates fast-oscillating quantities, and h.c. stands for the Hermitian conjugate). Here $\hat{A}_s^{(+)}$ and $\hat{A}_s^{(-)}$ represent the slowly varying envelopes of the positive- and negative-frequency components, respectively, of the electric field. We are seeking the functional dependence of these envelope functions on space and time. We can expand the envelope $\hat{A}_s^{(+)}$ in terms of photon annihilation operators $\hat{a}_j$, obeying the commutator $[\hat{a}_j, \hat{a}_k^{\dagger}] = \delta_{jk}$. In SI units,

$$\hat{A}_s^{(+)} = i\sum_j \mathscr{E}_j \hat{a}_j(t)\exp(-i\Omega_j t)\exp(iK_j z), \tag{4a}$$

$$\hat{A}_s^{(-)} = [\hat{A}_s^{(+)}]^{\dagger}, \tag{4b}$$

where $\mathscr{E}_j = (\hbar\omega_j/2\epsilon_j V)^{1/2}$, $\Omega_j = \omega_j - \omega_s$, $K_j = k_j - k_s$, $k_j = n_j\omega_j/c$, and $n_j = \sqrt{\epsilon_j/\epsilon_0}$ is the index of refraction at ω_j. We identify

$$\hat{E}(\omega_n) = i\mathscr{E}_n\hat{a}_n(t)\exp(ik_n z), \tag{5a}$$

noting that

$$\hat{E}(-\omega_n) = \hat{E}^{\dagger}(\omega_n). \tag{5b}$$

The interaction Hamiltonian $\hat{H}$ given by the field energy in the nonlinear medium is[58]

$$\hat{H} = \int_V \epsilon_0 {\sum_m}' \chi^{(2)}_{m,p-m}\hat{E}^{\dagger}(\omega_p)\hat{E}(\omega_m)\hat{E}(\omega_{p-m})\mathrm{d}^3 r + \text{h.c.}, \tag{6}$$

where $\chi^{(2)}_{m,p-m} = \chi^{(2)}(\omega_p, \omega_m, \omega_{p-m})$ and the prime on the summation indicates a sum over positive frequencies only ($m > 0$).

The pump field in $\hat{H}$ is given by

$$\hat{E}(\omega_p) = \exp(ik_p z)\hat{A}_p^{(+)}. \tag{7}$$

Putting these results into the interaction Hamiltonian in Eq. (6), we obtain for a medium of length L

$$\hat{H} = -\epsilon_0\hbar\chi^{(2)}\hat{A}_p^{(-)}{\sum_m}'' f_m\left[\frac{\omega_m(\omega_{p-m})}{\epsilon_m\epsilon_{p-m}}\right]^{1/2}\hat{a}_m\hat{a}_{p-m}$$

$$= -\epsilon_0\hbar\chi^{(2)}\hat{A}_p^{(+)}{\sum_m}'' f_m\left[\frac{\omega_m(\omega_{p-m})}{\epsilon_m\epsilon_{p-m}}\right]^{1/2}\hat{a}_m{}^{\dagger}\hat{a}_{p-m}{}^{\dagger}, \tag{8}$$

where $\chi^{(2)}$ is real and the double prime indicates that $0 < m < p/2$. The phase-matching function is

$$f_m = \left[\frac{\exp(-i\Delta k_m L) - 1}{-i\Delta k_m L}\right], \tag{9}$$

and the phase mismatch is given by

$$\Delta k_m = k_p - k_m - k_{p-m}. \tag{10}$$

Assuming a wide phase-matching bandwidth, $\Delta k_m \to 0$, we find that $f_m \to 1$. This result is realistic for typical crystals for which dispersion leads to a phase-matching bandwidth of the order of 10 THz.

This Hamiltonian demonstrates the intrinsic two-photon nature of parametric amplification. That is, the term proportional to $\hat{A}_p^{(+)}\hat{a}_p{}^{\dagger}a_{p-m}{}^{\dagger}$ indicates that the pump field is linked to the production of a photon at ω_m and a photon at ω_{p-m} (with the simultaneous annihilation of a pump photon at ω_p). In frequency space (see Fig. 1), the frequencies of the photon pairs are symmetric about half the pump frequency, $\omega_p/2$. Below, we discuss the phase-sensitive amplification that results from this Hamiltonian.

It is well known that Maxwell's wave equation is generated by Hamilton's equations of motion by use of the proper Hamiltonian and canonical dynamical variables. In quantum theory Hamilton's equations are replaced by Heisenberg's equations, which permits a greatly simplified direct route to the slowly varying wave propagation equation that we are seeking. Simple differentiation of Eq. (4a) gives

$$\left(\frac{\partial}{\partial z} + \frac{n_s}{c}\frac{\partial}{\partial t}\right)\hat{A}_s^{(+)} = i\sum_j \mathscr{E}_j\left[iK_j - i\frac{n_s}{c}\Omega_j + \frac{n_s}{c}\frac{\partial}{\partial t}\hat{a}_j(t)\right] \times \exp(-i\Omega_j t)\exp(iK_j z). \tag{11}$$

In Eq. (11) the first two terms on the right-hand side will cancel in the limit that $n_j \approx n_s$. The third term on the right-hand side is given by Heisenberg's equation of motion for any operator $\hat{O}$ and corresponding Hamiltonian $\hat{H}$:

$$\frac{\partial}{\partial t}\hat{O}(t) = \frac{i}{\hbar}[\hat{H}, \hat{O}(t)]. \tag{12}$$

Using the commutation relation

$$[\hat{a}_m\hat{a}_{p-m}, \hat{a}_j{}^{\dagger}] = \hat{a}_{p-m}\delta_{m,j} + \hat{a}_m\delta_{p-m,j} \tag{13}$$

(and remembering the requirement that $m < p/2$), we find the Heisenberg equation of motion for $\hat{a}_j{}^{\dagger}$ (in the interaction picture, where the linear free-field term in the Hamiltonian has been absorbed into the time dependence of $\tilde{E}$):

$$\frac{\partial}{\partial t}\hat{a}_j{}^{\dagger}(t) = -i\epsilon_0\chi^{(2)}\hat{A}_p^{(-)}\left(\frac{\omega_j\omega_{p-j}}{\epsilon_j\epsilon_{p-j}}\right)^{1/2}\hat{a}_{p-j}(t). \tag{14}$$

Substituting the Hermitian conjugate of Eq. (14) into Eq. (11), we obtain

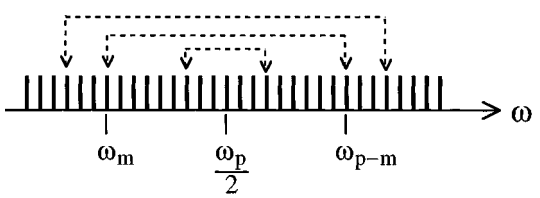

Fig. 1. Parametric amplification couples pairs of modes with frequencies symmetrically placed around one half of the pump frequency. A pair of photons at ω_m and ω_{p-m} is created when one pump photon is annihilated.

$$\left(\frac{\partial}{\partial z}+\frac{n_s}{c}\frac{\partial}{\partial t}\right)\hat{A}_s^{(+)}$$
$$=i\sum_j \mathscr{L}_j\left[iK_j-i\frac{n_s}{c}\Omega_j+\frac{n_s}{c}i\epsilon_0\chi^{(2)}\hat{A}_p^{(+)}\times\left(\frac{\omega_j\omega_{p-j}}{\epsilon_j\epsilon_{p-j}}\right)^{1/2}\hat{a}_{p-j}{}^{\dagger}(t)\right]\exp(-i\Omega_j t)\exp(iK_j z). \quad (15)$$

In typical experiments on degenerate parametric amplification or generation, squeezed intensity noise is measured in a small bandwidth (<100 MHz). In the case in which the medium is weakly dispersive over the small bandwidth of interest, centered at ω_s, we can approximate $\omega_j \approx \omega_{p-j} \approx \omega_s$ and $n_j \approx n_{p-j} \approx n_s$. The first two terms on the right-hand side cancel, and Eq. (15) becomes

$$\left(\frac{\partial}{\partial z}+\frac{n_s}{c}\frac{\partial}{\partial t}\right)\hat{A}_s^{(+)}(z,t)=\frac{-i\omega_s\chi^{(2)}}{cn_s}\hat{A}_p^{(+)}(z,t)\hat{A}_s^{(-)}(z,t). \quad (16)$$

With the usual transformation[51] to the moving frame coordinates, $\tau = t - n_s z/c$, Eq. (16) becomes

$$\frac{\partial}{\partial z}\hat{A}_s^{(+)}(z,\tau)=\frac{-i\omega_s\chi^{(2)}}{cn_s}\hat{A}_p^{(+)}(z,\tau)\hat{A}_s^{(-)}(z,\tau), \quad (17)$$

with τ held constant in $\partial/\partial z$. If we now treat the pump as a strong classical field that depends only on τ [replacing $\hat{A}_p^{(+)}(z,\tau)$ with $|A_p^{(+)}(\tau)|$], Eq. (17) can be solved explicitly. Combining Eq. (17) with the z derivative of its corresponding conjugate, we arrive at the equation

$$\frac{\partial^2}{\partial z^2}\hat{A}_s^{(+)}(z,\tau)=\kappa^2(\tau)\hat{A}_s^{(+)}(z,\tau), \quad (18)$$

where the coupling coefficient $\kappa(\tau)=\omega_s\chi^{(2)}|A_p^{(+)}(\tau)|/cn_s$.

We solve Eq. (18) to recover the equation of motion for the parametric amplifier with initial conditions $\hat{A}_s^{(+)}(0,\tau)$ and $\hat{A}_s^{(-)}(0,\tau)$. We obtain

$$\hat{A}_s^{(+)}(z,\tau)=\hat{A}_s^{(+)}(0,\tau)\cosh[\kappa(\tau)z]-i\hat{A}_s^{(-)}(0,\tau)\sinh[\kappa(\tau)z], \quad (19a)$$

$$\hat{A}_s^{(-)}(z,\tau)=\hat{A}_s^{(-)}(0,\tau)\cosh[\kappa(\tau)z]+i\hat{A}_s^{(+)}(0,\tau)\sinh[\kappa(\tau)z]. \quad (19b)$$

These are the fundamental equations for the degenerate parametric amplifier. They are functionally equivalent to Yuen's formulation for a single-mode field ($\hat{b}=\mu\hat{a}+\nu\hat{a}^{\dagger}$, with $|\mu|^2-|\nu|^2=1$).[7] Under the condition that the initial state corresponding to $\hat{A}_s^{(+)}(0,\tau)$ is the vacuum, the parametric amplifier leads to a squeezed vacuum, in which photon pairs reside.

Detection of squeezed light in experiments is typically accomplished by use of balanced homodyne detection, in which a strong LO field $f_{\mathrm{LO}}(t)\exp(-i\omega_s t)$ is interfered with the signal. The balanced homodyne detection measurement output is described by[51]

$$\hat{q}_\theta=\frac{1}{\sqrt{2}}[\hat{\alpha}\exp(-i\theta)+\hat{\alpha}^{\dagger}\exp(i\theta)], \quad (20)$$

where $\hat{\alpha}$ is the annihilation operator corresponding to the space–time mode defined by the overlap of the signal and the LO fields:

$$\hat{\alpha}=\frac{1}{\mathscr{L}_s}\int f_{\mathrm{LO}}(\tau)\hat{A}_s^{(+)}(L,\tau)\mathrm{d}\tau, \quad (21)$$

and θ is the LO's phase. The LO field is normalized such that $\int \mathrm{d}\tau|f_{\mathrm{LO}}(\tau)|^2=1$. We can then calculate the quadrature noise variance of the detected signal:

$$\Delta q_\theta{}^2=\langle\hat{q}_\theta{}^2\rangle-\langle\hat{q}_\theta\rangle^2=\langle\hat{q}_\theta{}^2\rangle. \quad (22)$$

With $\hat{q}_\theta$, given by Eqs. (20) and (21), we find that

$$\Delta q_\theta{}^2=(1/2)\int \mathrm{d}\tau|f_{\mathrm{LO}}(\tau)|^2\{\cosh[2\kappa(\tau)L]+\cos(2\theta)\sinh[2\kappa(\tau)L]\}. \quad (23)$$

It can be seen from this result that the maximum squeezing (reduction of $\Delta q_\theta{}^2$) occurs when $\cos(2\theta)=-1$ and when $f_{\mathrm{LO}}(\tau)$ has a duration much less than the duration of the gain parameter $\kappa(\tau)$ and $f_{\mathrm{LO}}(\tau)$ has its peak located at the peak of $\kappa(\tau)$.

The detected quadrature amplitude can also be defined in terms of a rotation

$$\hat{q}_\theta=\hat{Q}\cos\theta+\hat{P}\sin\theta, \quad (24)$$

such that $\hat{Q}=\hat{q}_{\theta=0}$ and $\hat{P}=\hat{q}_{\theta=\pi/2}$. The quadratures $\hat{Q}$ and $\hat{P}$ obey the uncertainty relation

$$\Delta Q\Delta P\geqslant 1/2, \quad (25)$$

with the equality holding for minimum-uncertainty states. The vacuum [obtained when $\kappa\to 0$ in Eq. (23)], or any other coherent state, has quadratures with equal uncertainty:

$$\Delta Q^2=\Delta P^2=1/2. \quad (26)$$

When the LO pulse $f_{\mathrm{LO}}(\tau)$ is much shorter in duration than $\kappa(\tau)$, a squeezed state will have variances given by, for example,

$$\Delta Q^2=(1/2)\exp[-2s(\tau_{\mathrm{LO}})], \quad (27a)$$

$$\Delta P^2=(1/2)\exp[2s(\tau_{\mathrm{LO}})], \quad (27b)$$

where τ_{LO} is the time of the LO pulse maximum and where we have introduced the squeezing gain parameter $s(\tau)=\kappa(\tau)L$. Squeezing is defined as the uncertainty in one quadrature dropping below the vacuum, or shot-noise, level; e.g., $\Delta Q^2<1/2$. Before the advent of squeezing experiments, the shot-noise level was generally thought to be a lower bound in optical detection. With squeezing, however, this variance can theoretically approach zero (100% squeezing) for infinite gain.

One is often interested in characterizing the gain parameter s without doing a squeezing experiment. Fortunately, this gain is the same gain that appears in parametric optical amplification. Parametric amplification can occur when a weak seed beam at frequency ω_s and a strong pump beam at frequency $\omega_p=2\omega_s$ enter a $\chi^{(2)}$ nonlinear crystal. The weak probe beam can be amplified or deamplified, depending on the relative phase ϕ between the seed beam and the pump beam. For a single-mode field entering a parametric amplifier, the

parametric amplification (or gain) factor G of the seed (output flux/input flux) can be found from Eqs. (19) to be[59]

$$G(\tau) = \cosh[2s(\tau)] - \cos\,\phi\,\sinh[2s(\tau)]. \tag{28}$$

By varying ϕ, we can obtain the maximum and minimum amplification, given by

$$G_{\max}(\tau) = \exp[2s(\tau)], \tag{29a}$$

$$G_{\min}(\tau) = \exp[-2s(\tau)], \tag{29b}$$

where we have assumed perfect phase matching and spatial overlap between the pump and the seed beams. Comparing Eqs. (29) with Eqs. (27), we can see that the maximum amount of squeezing obtainable is directly proportional to the maximum amount of deamplification in the parametric amplifier. If we can deamplify the seed by 50%, we can, in principle (assuming perfect detection efficiency), obtain 50% squeezing.

Even a classical parametric amplifier has gain at ω_s, half the frequency of the pump. The phase sensitivity of the gain is what leads to the reduction of one quadrature and the increase of the other. The quantum nature of the field allows for seeding of the field at ω_s by spontaneous two-photon emission as well as for the quantum correlations needed for sub-shot-noise light detection.

In the absence of perfect detection efficiency, however, the squeezing is degraded because the squeezing process depends on the production of twin photons (pairs of photons created simultaneously). Losses introduce a random deletion of individual photons, thus destroying the quantum correlation within photon pairs. The detection efficiency comprises several factors. Detector quantum efficiency, transmission of optical components, and spatial mode matching can be accounted for by the detection efficiency η_{det} (which lies between 0 and 1). The measured amount of squeezing will be degraded[44,52,59] such that

$$(\Delta q_\theta^{\,2})_{\text{measured}} = (1/2)[1 - \eta_{\text{det}} + \eta_{\text{det}}(\Delta q_\theta^{\,2})_{\text{produced}}], \tag{30}$$

where $(\Delta q_\theta^{\,2})_{\text{produced}}$ is given by Eq. (23). Thus, if our efficiency is 40% and we generate a perfect squeezed state, we will still observe only 40% squeezing.

A further consideration is temporal mode matching. In pulsed squeezing experiments the effects of temporal overlap between the LO and the squeezed signal affect the overall efficiency and the effective parametric gain coefficient s_{eff}.[60] A phenomenological expression for the rotated quadrature variance is given by[52]

$$\Delta q_\theta^{\,2} = \frac{1}{2} + \frac{\eta_{\text{det}}\eta_{\text{temp}}}{2}[\cosh(2s_{\text{eff}}) - 1 + \cos(2\theta)\sinh(2s_{\text{eff}})]. \tag{31}$$

By fitting this formula to the experimental squeezing results we extract the effective gain coefficient s_{eff} and the product $\eta_{\text{det}}\eta_{\text{temp}}$, where η_{temp} is the effective temporal mode-matching efficiency (which lies between 0 and 1).

5. $LiTaO_3$ WAVEGUIDES

The channel waveguides with periodic domain inversion were made at the Eastman Kodak Company in Rochester, New York. We provide a short description of the patterning technique here. A more detailed description of the formation process is given by Baron *et al.*[61] The quasi-phase-matched channel waveguides in this study were fabricated in an optical grade z-cut $LiTaO_3$ crystal wafer by proton exchange, followed by the application of a uniform electric field to generate domain inversion for QPM.

The fabrication process involves several steps. First, a Ta mask with 3.6-μm period is laid onto the bulk crystal. The crystal is then soaked in pyrophosphoric acid to permit proton exchange. The protons diffuse through the rectangular open regions in the mask and replace the Li ions. After proton exchange is complete, the Ta mask is removed and the crystal is placed in a uniform electric field of ~22 kV/mm. The electric field flips the direction of the spontaneous polarization in the unexchanged regions, leaving the p-exchanged regions unperturbed. This periodic poling leads to a structure that supports QPM and greatly enhances the SHG efficiency.[48] The final step is to create the channel waveguide in this periodically poled bulk crystal in a direction transverse to the domain grating. Another Ta mask with a 4-μm-wide channel is laid onto the crystal and is then p exchanged in the pyrophosphoric acid. The p-exchanged region has a higher index of refraction than the bulk crystal, thus forming a waveguide. Fabrication was completed with polishing of the ends of the waveguides to optical quality. The waveguides were then annealed at 380 °C and showed a single IR mode at 840 nm. These waveguides can have SHG efficiencies as much as 3 orders of magnitude beyond those of bulk doubling crystals. The waveguides used in this study have a SHG conversion efficiency of ~30% for a train of picosecond pulses.[62] The magnitude of the nonlinear coefficient $|d_{33}|$ for $LiTaO_3$ is 21 pm/V (at 1.06 μm). For comparison, $KTiOPO_4$ and $LiNbO_3$ have $|d_{33}|$ coefficients of 13.7 and 34.4 pm/V, respectively.[63]

6. SQUEEZING

The experimental apparatus for squeezing is shown in Fig. 2. We start with a Ti:sapphire chirped-pulse regenerative amplifier laser system generating pulses at 1 kHz, centered at wavelength 840 nm, with a temporal duration variable from 150 fs to 3 ps and a pulse energy of ~1 μJ. The laser beam is split into two arms at the first polarizing beam splitter (PBS1). The lower arm becomes our LO; the upper arm will generate our signal. The seed arm is blocked for this measurement. First we generate our pump at 420 nm by frequency doubling the red light in a 5-mm-long, type I LiB_3O_5 (LBO) doubling crystal. We block the residual red light with a blue filter and then focus the pump into the waveguide (WG1) with a blue antireflection-coated diode laser lens (DL_b). The down-conversion signal produced in the waveguide is then collimated with a red-coated diode lens (DL_r) and propagates to polarizing beam splitter PBS2, where it will spatially overlap our LO. (The seed beam, indicated in

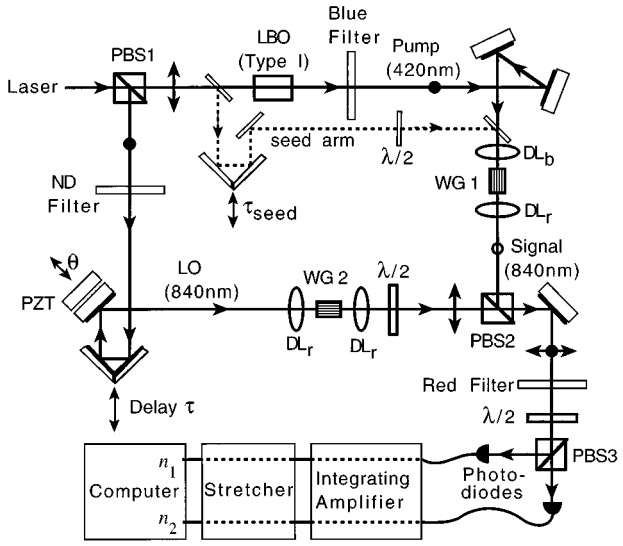

Fig. 2. Schematic of squeezing experiment. The seed arm is used only for study of blue-light-induced red absorption.

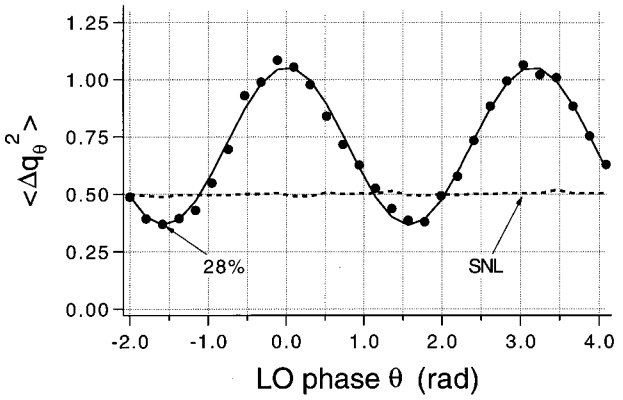

Fig. 3. Squeezed quadrature variance versus LO phase. Filled circles, data; solid curve, fit to Eq. (31) with $\eta_{\mathrm{det}}\eta_{\mathrm{temp}} = 0.36$ and $s_{\mathrm{eff}} = 0.71$; dashed curve, shot-noise level.

Fig. 2 by the topmost dashed line, is used in an independent experiment to measure the blue-light-induced red absorption; see below.) In the lower arm the LO is attenuated with a neutral-density (ND) filter, delayed temporally by amount τ in a variable-delay line, and then phase shifted by θ via a mirror attached to a piezoelectric translator (PZT). The LO is then put through a dummy waveguide (WG2) to ensure proper spatial mode matching to the signal.

The LO and the signal (orthogonally polarized to each other) are spatially overlapped at PBS2 and propagate collinearly to a balanced homodyne detector. First a red filter blocks any remaining pump light; then a half-wave plate ($\lambda/2$) rotates the beams to 45°, and polarizing beam splitter PBS3 mixes and splits the two signals. The $\lambda/2$ plate and PBS3 constitute our 50/50 beam splitter, which is necessary for balanced homodyne detection.[9,11,49,50] The orientation of the $\lambda/2$ plate is controlled by an extremely high-precision rotation stage. The precise rotation of the $\lambda/2$ plate is crucial to obtaining a true 50/50 split, which is more important in dc-balanced homodyne detection, used here, than it is in rf-homodyne detection, as is more commonly employed. The resulting beams are then focused onto a pair of photodiodes by short-focal-length lenses. The focused spot size is smaller than the detector area to ensure little loss of light. The high-efficiency photodiodes have response times much longer ($\sim$2 ns) than the pulse durations. The photocurrents are integrated in charge-sensitive amplifiers whose outputs are sampled by analog-to-digital converters, to yield pulse photoelectron numbers $\hat{n}_1$ and $\hat{n}_2$. For specifics on the electronics, see Ref. 64. The difference number $\hat{N}_{12} = \hat{n}_1 - \hat{n}_2$ is proportional to the quadrature amplitude $\hat{q}_\theta$, as defined in Eq. (20).

Our best squeezing results occur when picosecond pulses are used; these results are shown in Fig. 3. The quadrature variance is plotted versus the LO phase varied by use of the PZT. The experimental data are indicated by the filled circles; the solid curve is a fit based on Eq. (31) with $\eta_{\mathrm{det}}\eta_{\mathrm{temp}} = 0.36$, $s_{\mathrm{eff}} = 0.71$, and the dashed curve represents the vacuum shot-noise level, measured independently (determining the shot-noise level uses the same procedure as determining $|\alpha_{\mathrm{LO}}|$ above; see Ref. 64). In this experiment the LO contained roughly 800,000 photons, the LO pulse duration was 1 ps, the pump pulse duration was $\sim$2 ps, and the input pump pulse energy at $z = 0$ was 0.4 nJ. The gain seen in squeezing ($s_{\mathrm{eff}} = 0.71$) is in rough agreement with the waveguide efficiencies measured from an independent SHG measurement (see Ref. 62). Noise below the shot-noise level is clearly seen at certain phase values with a minimum quadrature variance of 0.36, which corresponds to a squeezing level of 28%.

The state is not a minimum-uncertainty state because of the poor detection efficiency, as indicated by the large rise of noise to 1.08 at the peaks. This low detection efficiency was perplexing because the passive losses in the system are small. The photodiodes have a quantum efficiency of 93%. The optical components from the waveguide to the detectors have a transmission of 93%. The spatial mode matching is 87% as measured by classical interference contrast. The temporal mode-matching efficiency η_{temp}, calculated from the temporal pulse profiles,[52] is greater than 95%, since group-velocity walk-off in our doubling crystal generates a pump pulse that is at least twice as long as the LO pulse. These factors lead to an overall detection efficiency $\eta_{\mathrm{det}}\eta_{\mathrm{temp}}$ of 71%, yet our squeezing levels indicate an efficiency of 36%. This discrepancy led us to study another loss mechanism in the waveguides: blue-light-induced red absorption.

7. MODEL FOR BLUE-LIGHT-INDUCED RED ABSORPTION

Blue-light-induced red absorption (BLIRA) is the attenuation of a red probe beam in the presence of strong blue light. BLIRA, also known as blue-light-induced infrared absorption (BLIIRA),[65] is detrimental to the performance of nonlinear optical crystals. In a nonlinear optical waveguide the effect is readily active because of the high intensities and long interaction lengths. In bulk crystals it has degraded achievable squeezing in optical paramet-

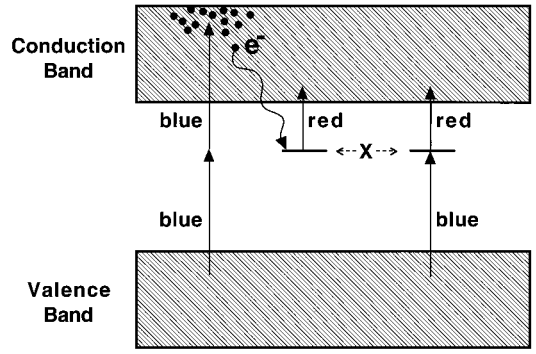

Fig. 4. Physical model for blue TPA and the generation of trap states X for BLIRA.

ric oscillation[32,66] and limited SHG in high-power single-pass $KNbO_3$.[67] Shiv *et al.*[68] have investigated methods for circumventing BLIIRA in $KNbO_3$ by using higher temperatures, longer wavelengths, and different cuts of the crystal. Their results are encouraging to the nonlinear optics community.

BLIIRA was previously modeled by assuming the existence of several free-carrier trapping states.[69] The physical model for BLIRA that we present here is based on blue TPA[70] into the conduction band of the crystal and the subsequent population of trap states. The model is shown in Fig. 4. Single photons of blue light are absorbed near the semiconductor band edge, where presumably trap states exist. Single-photon absorption (SPA) and TPA of strong blue pump light are modeled according to

$$\frac{dI_b}{dz} = -\alpha_b I_b - \beta_b {I_b}^2, \tag{32}$$

where I_b is the blue intensity (W/cm^2), z is the propagation distance (along the waveguide), and α_b and β_b are the blue SPA and TPA coefficients, respectively. Solving this equation, we find for the transmitted intensity $I_b(L, t) = T_b(t) I_b(0, t)$, where $T_b(t)$ is the blue transmission[71]:

$$T_b(t) = \left\{ I_b(0, t) \frac{\beta_b}{\alpha_b} [\exp(\alpha_b L) - 1] + \exp(\alpha_b L) \right\}^{-1}, \tag{33}$$

where $I_b(0, t)$ is the intensity at the input face at time t and L is the length of the waveguide. Assuming a sech^2 pulse shape for $I_b(0, t) = I_0 \operatorname{sech}^2(1.76t/\tau)$, where τ is the FWHM of the input blue-pulse intensity, we can integrate analytically over all time to solve for the transmitted pulse energy E_{out} as a function of input energy E_{in}:

$$E_{\text{out}} = \frac{E_{\text{in}} \exp(-\alpha_b L)}{2\sqrt{u(u+1)}} \ln\left[\frac{\left(1 + \frac{1}{u}\right)^{1/2} + 1}{\left(1 + \frac{1}{u}\right)^{1/2} - 1} \right], \tag{34}$$

where

$$u = \frac{1.76 E_{\text{in}} \beta_b}{A_{\text{wg}} \tau \alpha_b} [1 - \exp(-\alpha_b L)] \tag{35}$$

and A_{wg} is the cross-sectional area of the waveguide. Note that Eq. (32) neglects absorption of blue light by blue-generated trapped carriers.[70]

The trap states are assumed to be generated by both single-photon and two-photon blue absorption, according to

$$\frac{dN_x}{dt} = \frac{1}{\hbar\omega} \alpha_b I_b + \frac{\xi}{2\hbar\omega} \beta_b {I_b}^2, \tag{36}$$

where N_x is the number density of trap states X, $\hbar\omega$ is the energy of the blue photon, and ξ is the probability that an electron in the conduction band will get caught at a trap site. These traps can then absorb red light by SPA according to

$$\frac{dI_r}{dz} = -\sigma_x N_x I_r, \tag{37}$$

where I_r is the red-light intensity and σ_x is the red absorption cross section for the trap state. (Also, we have neglected any single-photon and two-photon red absorption by the material in the absence of blue light, because the material is essentially transparent at the red wavelength.) The end result of this whole process is greater attenuation of the red beam with increasing blue pump energy.

8. EXPERIMENTAL TWO-PHOTON ABSORPTION AND BLUE-LIGHT-INDUCED RED ABSORPTION

To measure the TPA of the blue pump pulse we monitored the output blue energy through the waveguide as we increased the blue energy entering the waveguide. The results are shown in Fig. 5, where we have plotted the blue-energy transmission $E_{\text{out}}/E_{\text{in}}$ of the waveguide as a function of blue energy at $z = 0$. To calculate the blue energy at $z = 0$ we measured the energy of the blue light before the waveguide and estimated a waveguide coupling efficiency of 22%. The blue transmission drops quickly with increasing energy and then levels off at a value of ~6% at an input energy of 2.9 nJ. The damage threshold for $LiTaO_3$ was found to be ~40 nJ (incident upon the waveguide face). The solid curve in Fig. 5 is the

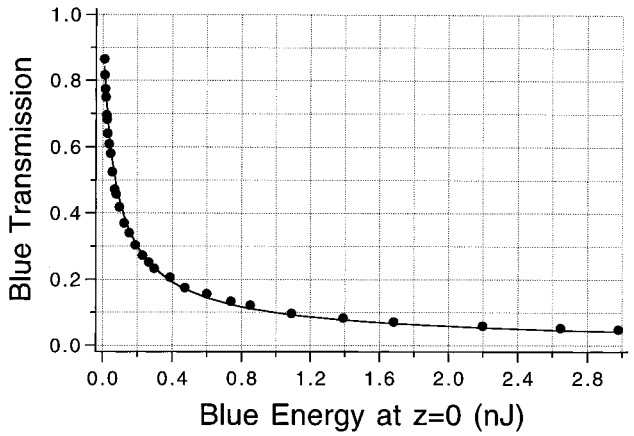

Fig. 5. TPA of blue light in a $LiTaO_3$ waveguide. Here we plot the transmission of a blue pulse versus input blue energy.

theory based on our model, Eq. (34), with $A_{wg} = 8 \times 10^{-8}$ cm^2 and $\tau = 1$ ps; the data are indicated by the filled circles. Fixing the linear absorption to a value $\alpha_b = 0.07$ cm^{-1} and varying β_b, we obtained a good fit to the data with a value for the TPA coefficient $\beta_b = 2.2 \times 10^{-9}$ cm/W. This value could be off by 50%, however, because of the sensitivity of the model to waveguide coupling efficiency. Nonetheless, this value is more than an order of magnitude greater than those found in optical fibers ($\sim 1 \times 10^{-10}$ cm/W).

The experimental arrangement for measuring BLIRA is shown in Fig. 2. The two lower dashed lines indicate the red seed beam used to probe the waveguide, temporally delayed from the blue pump pulse by τ_{seed}. By varying τ_{seed} we could probe the turn-on time of the BLIRA and found that it is essentially instantaneous (as fast as our shortest pump pulse, ~250 fs), yet the effect survives as long as a millisecond. We measured the red transmitted energy $E_r(L, E_{in})$ as a function of blue input energy E_{in}. The results are shown in Fig. 6, where we have plotted the BLIRA absorption factor A_r [1 minus the red transmitted energy $E_r(L, E_{in})$ in the presence of blue light divided by the red transmitted energy $E_r(L, 0)$ without blue light] versus input blue pump energy E_{in}:

$$A_r(E_{in}) = 1 - \frac{E_r(L, E_{in})}{E_r(L, 0)}. \tag{38}$$

We observed nearly 50% absorption of the red beam at high pump energies. This result agrees qualitatively with our squeezing results, for which we found that the detection efficiency (the fitted value of $\eta_{det}\eta_{temp}$) went down with increasing pump energy.

Equations (36) and (37) are sufficient to fit the data shown in Fig. 6; however, the theory predicts a dependence on blue-pulse duration that contradicts our preliminary experimental results (i.e., with $\xi = 0.016$ and $\sigma_x = 6.0 \times 10^{-17}$ cm^2, the theory predicts that 10-ps pulses will generate more BLIRA than 1-ps pulses, opposite what we found experimentally). We are currently working on unraveling this discrepancy and hope to present a fully consistent model in a future publication.

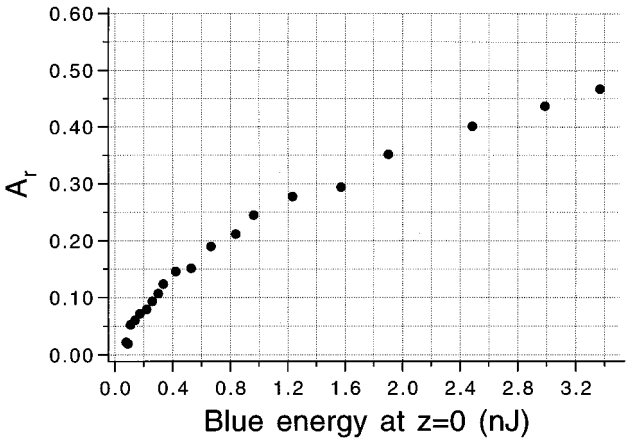

Fig. 6. BLIRA in a $LiTaO_3$ waveguide. Here we plot the BLIRA factor A_r [1 minus the red transmitted energy $E_r(L, E_{in})$ in the presence of blue light divided by the red transmitted energy $E_r(L,0)$ without blue light] from Eq. (38) as a function of input blue energy.

9. SUMMARY AND CONCLUSIONS

The deleterious effects of two-photon absorption (TPA) and blue-light-induced red absorption (BLIRA) indicate that ultrafast pulses in nonlinear optical waveguides might not be capable of generating large amounts of squeezing at these wavelengths. The problem is that TPA quickly attenuates the amount of blue pump light available for squeezing, thus limiting the squeezing gain, whereas BLIRA induces absorptive losses for the red light, thus destroying squeezed light's quantum correlations between photon pairs. This situation is typical of the trade-offs that are often present in nonlinear optics, and possible circumventions do exist. For instance, the blue pump frequency could be lowered to operate below half-band-gap of the $LiTaO_3$ crystal, thus preventing TPA. QPM devices are particularly suited to operation over a range of frequencies inaccessible to birefringent phase matching; thus this could be an attractive match. Another proposition that warrants investigation is the use of longer pump pulses to effectively lower the peak intensity, thus limiting the amount of TPA. (The caveat with longer pulses, however, is that one must still be able to generate a short LO for pulsed homodyne detection. Generating such a combination of long and short pulses is difficult but feasible.) With high-efficiency waveguides, longer pulses could still generate considerable squeezing.

As Kimble pointed out,[44] there has been noticeable lack of systematic progress in the experiments since 1985. The amount of squeezing does not linearly improve with time, as one might expect, but jumps around rather randomly. This behavior stems from the pursuit of a simple system to produce squeezed light. Nonlinear optical waveguides simplify the squeezing process in some respects and, if the BLIRA can be overcome, may provide a new means to generate large amounts of squeezing. It remains to be seen what the fundamental limiting factor that limits the squeezing will be. TPA of blue light may occur and lead to red absorption; linear absorption of red light cannot be entirely eliminated; and Kerr effects and nonlinear modification of wave guiding can occur at high pump powers.

ACKNOWLEDGMENTS

We acknowledge the generous support and friendship of John Bierlein, who passed away recently. His continued contribution to optics will be greatly missed.

This research was supported by the National Science Foundation, Division of Atomic, Molecular, and Optical Physics.

REFERENCES AND NOTES

1. E. Schrödinger, Naturwissenschaften **14**, 664 (1926).
2. R. J. Glauber, in *Quantum Optics and Electronics* (Les Houches Summer School of Theoretical Physics, University of Grenoble), C. DeWitt, A. Blandin, and C. Cohen-Tannoudji, eds. (Gordon & Breach, New York, 1965), p. 63.

3. J. N. Hollenhorst, Phys. Rev. D **19**, 1669 (1979).
4. W. H. Louisell, A. Yariv, and A. E. Siegman, Phys. Rev. **124**, 1646 (1961).
5. H. Takahasi, in *Advances in Communications Systems*, A. Balakrishnan, ed. (Academic, New York, 1965), Vol. 1, pp. 237–310.
6. D. Stoler, Phys. Rev. D **1**, 3217 (1970); **4**, 1925 (1971).
7. H. P. Yuen, Phys. Rev. A **13**, 2226 (1976).
8. C. Caves, Phys. Rev. D **23**, 1693 (1981).
9. R. E. Slusher, L. W. Hollberg, B. Yurke, J. C. Mertz, and J. F. Valley, Phys. Rev. Lett. **55**, 2409 (1985); R. E. Slusher, B. Yurke, P. Grangier, A. LaPorta, D. F. Walls, and M. Reid, J. Opt. Soc. Am. B **4**, 1453 (1987).
10. R. M. Shelby, M. D. Levenson, S. H. Perlmutter, R. G. DeVoe, and D. F. Walls, Phys. Rev. Lett. **57**, 691 (1986).
11. L. A. Wu, H. J. Kimble, J. L. Hall, and H. Wu, Phys. Rev. Lett. **57**, 2520 (1986); L. A. Wu, M. Xiao, and H. J. Kimble, J. Opt. Soc. Am. B **4**, 1465 (1987).
12. M. W. Maeda, P. Kumar, and J. H. Shapiro, Opt. Lett. **12**, 161 (1987).
13. M. G. Raizen, L. A. Orozco, M. Xiao, T. L. Boyd, and H. J. Kimble, Phys. Rev. Lett. **59**, 198 (1987); L. A. Orozco, M. G. Raizen, M. Xiao, R. J. Brecha, and H. J. Kimble, J. Opt. Soc. Am. B **4**, 1490 (1987).
14. B. L. Schumaker, S. H. Perlmutter, R. M. Shelby, and M. D. Levenson, Phys. Rev. Lett. **58**, 357 (1987).
15. P. Grangier, R. E. Slusher, B. Yurke, and A. LaPorta, Phys. Rev. Lett. **59**, 2153 (1987).
16. R. E. Slusher, P. Grangier, A. LaPorta, B. Yurke, and M. J. Potasek, Phys. Rev. Lett. **59**, 2566 (1987).
17. S. F. Pereira, M. Xiao, H. J. Kimble, and J. L. Hall, Phys. Rev. A **38**, 4931 (1988).
18. S. F. Pereira, K. C. Peng, and H. J. Kimble in *Coherence and Quantum Optics VI*, J. H. Eberly, L. Mandel, and E. Wolf, eds. (Plenum, New York, 1990), p. 889.
19. S.-T. Ho, N. C. Wong, and J. H. Shapiro, in *Coherence and Quantum Optics VI*, J. H. Eberly, L. Mandel, and E. Wolf, eds. (Plenum, New York, 1990), p. 497.
20. P. Kumar, O. Aytür, and J. Huang, Phys. Rev. Lett. **64**, 1015 (1990).
21. A. Sizmann, R. J. Horowicz, E. Wagner, and G. Leuchs, Opt. Commun. **80**, 138 (1990).
22. R. Movshovich, B. Yurke, P. G. Kaminsky, A. D. Smith, A. H. Silver, R. W. Simon, and M. V. Schneider, Phys. Rev. Lett. **65**, 1419 (1990).
23. T. Hirano and M. Matsuoka, Opt. Lett. **15**, 1153 (1990).
24. M. Rosenbluh and R. M. Shelby, Phys. Rev. Lett. **66**, 153 (1991).
25. K. Bergman and H. A. Haus, Opt. Lett. **16**, 663 (1991).
26. S. T. Ho, N. C. Wong, and J. H. Shapiro, Opt. Lett. **16**, 840 (1991).
27. O. Aytür and P. Kumar, Opt. Lett. **17**, 529 (1992).
28. D. M. Hope, H. A. Bachor, P. J. Manson, D. E. McClelland, and P. T. H. Fisk, presented at the Tenth International Conference on Laser Spectroscopy, Font-Romeu, France, June 17–21, 1991.
29. P. Kurz, R. Paschotta, K. Fiedler, A. Sizmann, G. Leuchs, and J. Mlynek, Appl. Phys. B **55**, 216 (1992).
30. R. M. Shelby and M. Rosenbluh, Appl. Phys. B **55**, 226 (1992).
31. T. Hirano and M. Matsuoka, Appl. Phys. B **55**, 233 (1992).
32. E. S. Polzik, J. Carri, and H. J. Kimble, Appl. Phys. B **55**, 279 (1992).
33. D. T. Smithey, M. Beck, M. G. Raymer, and A. Faridani, Phys. Rev. Lett. **70**, 1244 (1993).
34. K. Bergman, C. R. Doerr, H. A. Haus, and M. Shirasaki, Opt. Lett. **18**, 643 (1993).
35. N. Nishizawa, S. Kume, M. Mori, T. Goto, and A. Mayauchi, Jpn. J. Appl. Phys. **33**, 138 (1994).
36. K. Bergman, H. A. Haus, E. P. Ippen, and M. Shirasaki, Opt. Lett. **19**, 290 (1994).
37. C. Kim and P. Kumar, Phys. Rev. Lett. **73**, 1605 (1994); C. Kim, R.-D. Li, and P. Kumar, Opt. Lett. **19**, 132 (1994).
38. A. M. Fox, J. J. Baumberg, M. Dabbicco, B. Huttner, and J. F. Ryan, Phys. Rev. Lett. **74**, 1728 (1995).
39. M. E. Anderson, M. Beck, M. G. Raymer, and J. D. Bierlein, Opt. Lett. **20**, 620 (1995).
40. D. K. Serkland, M. M. Fejer, R. L. Byer, and Y. Yamamoto, Opt. Lett. **20**, 1649 (1995).
41. G. Breitenbach, T. Muller, S. F. Pereira, J.-P. Poizat, S. Schiller, and J. Mlynek, J. Opt. Soc. Am. B **12**, 2304 (1995).
42. A. M. Fox, M. Dabbicco, G. von Plessen, and J. F. Ryan, Opt. Lett. **20**, 2523 (1995).
43. A. Lambrecht, T. Coudreau, A. M. Steinberg, and E. Giacobino, Europhys. Lett. **36**, 93 (1996).
44. H. J. Kimble, Phys. Rep. **219**, 227 (1992). See also H. J. Kimble, *Systemes Fondamentaux en Optique Quantique (Fundamental Systems in Quantum Optics)*, J. Dalibard, J.-M. Raimond, and J. Zinn-Justin, eds. (Elsevier, Amsterdam, 1992), pp. 545–669.
45. A. LaPorta and R. E. Slusher, Phys. Rev. A **44**, 2013 (1991).
46. S.-T. Ho, X. Zhang, and M. K. Udo, J. Opt. Soc. Am. B **12**, 1537 (1995).
47. P. Kumar, in *Squeezed and Nonclassical Light*, P. Tombesi and E. R. Pike, eds. (Plenum, New York, 1988), p. 175.
48. M. M. Fejer, Phys. Today **47**(5), 25 (1994); M. M. Fejer, G. A. Magel, D. H. Jundt, and R. L. Byer, IEEE J. Quantum Electron. **28**, 2631 (1992).
49. H. P. Yuen and V. W. S. Chan, Opt. Lett. **8**, 177 (1983).
50. M. G. Raymer, J. Cooper, H. J. Carmichael, M. Beck, and D. T. Smithey, J. Opt. Soc. Am. B **12**, 1801 (1995).
51. B. Yurke, P. Grangier, R. E. Slusher, and M. J. Potasek, Phys. Rev. A **35**, 3586 (1987).
52. D. T. Smithey, M. Beck, J. Cooper, and M. G. Raymer, Phys. Scr. **T48**, 35 (1993). We discovered a missing factor of 2 in this reference; namely, $s(t)$ in Eq. (20) should be replaced by $2s(t)$, and s_{eff} in Eq. (23) should be replaced by $2s_{\mathrm{eff}}$.
53. M. J. Werner, M. G. Raymer, M. Beck, and P. D. Drummond, Phys. Rev. A **52**, 4202 (1995).
54. I. P. Christov, V. D. Stoev, M. M. Murnane, and H. C. Kapteyn, Opt. Lett. **21**, 1493 (1996).
55. M. G. Roelofs, A. Suna, W. Bindloss, and J. D. Bierlein, J. Appl. Phys. **76**, 4999 (1994).
56. D. K. Serkland, P. Kumar, M. A. Arbore, and M. M. Fejer, presented at the Optical Society of America Annual Meeting, Rochester, New York, (1996); in *Quantum Communication, Computing, and Measurement*, O. Hirota, A. S. Holevo, and C. M. Caves, eds. (Plenum, New York, to be published).
57. R. Loudon and P. L. Knight, J. Mod. Opt. **34**, 709 (1987).
58. R. W. Boyd, *Nonlinear Optics* (Academic, San Diego, Calif., 1992).
59. P. D. Townsend and R. Loudon, Phys. Rev. A **45**, 458 (1992).
60. In Ref. 52 s_{eff} is the squeezing gain parameterized by the time-dependent gain $s(\tau)$ and the LO and pump pulse temporal profiles.
61. C. Baron, H. Cheng, and M. Gupta, Appl. Phys. Lett. **68**, 481 (1996); V. Gopalan and M. Gupta, J. Appl. Phys. **80**, 6099 (1996).
62. This conversion efficiency was measured in a SHG experiment by means of a 1-kHz pulse train with 840-fs pulses at an energy of 60 pJ. This absolute conversion efficiency represents the output blue energy divided by the input red energy. Typically, waveguide SHG efficiencies are characterized in units of percent per (watts times square centimeters). Multiplying this number by the fundamental power and the square of the waveguide length gives the second-harmonic power. With ultrashort pulses, however, the effective length of the device is determined by group-velocity walk-off between the fundamental and the second harmonic. Taking walk-off effects into consideration, we calculate an efficiency of 3%/W cm^2 for these devices. From the squeezing experiment we calculate an efficiency of 1.2%/W cm^2. However, cw SHG results obtained by other groups of researchers indicate higher efficiencies, 100–300%/W cm^2; see Ref. 55 or 61.
63. V. G. Dmitriev, G. G. Gurzadyan, and D. N. Nikogosyan, *Handbook of Nonlinear Optical Crystals* (Springer-Verlag, Berlin, 1991).
64. M. E. Anderson, M. Munroe, U. Leonhardt, D. Boggavarapu, D. F. McAlister, and M. G. Raymer, in *Generation,*

Amplification, and Measurement of Ultrafast Laser Pulses III, W. E. White and D. H. Reitze, eds., Proc. SPIE **2701**, 142 (1996).
65. E. S. Polzik and H. J. Kimble, in *Inorganic Crystals for Optics, Electro-Optics, and Frequency Conversion*, P. F. Bordui, ed., Proc. SPIE **1561**, 143 (1991).
66. E. S. Polzik, J. Carri, and H. J. Kimble, Phys. Rev. Lett. **68**, 3020 (1992).
67. L. E. Busse, L. Goldberg, M. R. Surette, and G. Mizell, J. Appl. Phys. **75**, 1102 (1993).
68. L. Shiv, J. L. Sørensen, E. S. Polzik, and G. Mizell, Opt. Lett. **20**, 2270 (1995).
69. H. Mabuchi, E. S. Polzik, and H. J. Kimble, J. Opt. Soc. Am. B **11**, 2023 (1994).
70. E. W. Van Stryland, H. Vanherzeele, M. A. Woodall, M. J. Soileau, A. L. Smirl, S. Guha, and T. F. Boggess, Opt. Eng. **24**, 613 (1985); A. Villeneuve, C. C. Yang, G. I. Stegeman, C. N. Ironside, G. Scelsi, and R. M. Osgood, IEEE J. Quantum Electron. **30**, 1172 (1994).
71. T. Mizunami, M. Hashimoto, M. Yamashiro, S. Gupta, and T. Shimomura, in *Nonlinear Guided Waves and Their Applications*, Vol. 15 of 1996 OSA Technical Digest Series (Optical Society of America, Washington, D.C., 1996), pp. 233–235.